Verification, validation, and cross-comparison of tritium transport codes FESTIM, MHIMS, and mHIT

Nuclear Materials and Energy 45 (2025) 102026

Contents lists available at ScienceDirect

Nuclear Materials and Energy

journal homepage: www.elsevier.com/locate/nme

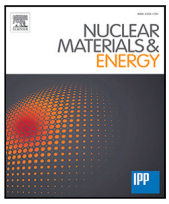

Verification, validation, and cross-comparison of tritium transport codes FESTIM, MHIMS, and mHIT☆

Gabriele Ferrero [a], Raffaella Testoni [a,*], Etienne A. Hodille [b]

[a] Politecnico di Torino, Dipartimento di Energia "Galileo Ferraris", Corso Duca degli Abruzzi 24, Turin, Italy
[b] CEA, IRFM/GCFPM, F-13108 Saint-Paul-lez-Durance, France

ARTICLE INFO

Dataset link: https://github.com/gabriele-ferrero/Titans_TT_codecomparison

Keywords:
Hydrogen isotopes transport
Tritium
Finite element
Modeling
Nuclear fusion

ABSTRACT

Tritium transport is a fundamental topic in the development of nuclear fusion reactors for sustainable and competitive energy production. Tritium breeding blankets and extraction systems must be as efficient as possible. Tritium handling systems are crucial to ensure fuel self-sufficiency, safe operations, and cost reduction. Component-level modeling supports design choices to build a more efficient system. In recent years, multiple component-level codes dedicated to simulating hydrogen Isotope transport mechanisms, such as permeation across materials and trapping, have been developed, verified, and validated. This work presents a comparison between three codes, MHIMS, FESTIM, and mHIT, in different verification and validation benchmarks, and their application on the ITER tungsten monoblock. The code comparison includes the V&V study for the mHIT code, and FESTIM results are compared against another code for the ITER monoblock in 2D and during transients. Indeed, to analyze and design tritium components for a fusion power plant, such as a breeder blanket, a plethora of features are necessary, such as trapping, 3 dimensions, multi-material interfaces, time-dependent transients, chemical reactions, and CFD coupling. The benchmarks showcased good agreement between the codes and experimental results. This work demonstrates the coherence and the solid common ground between the codes, verifies some features that are already implemented, and can serve as a starting point for more complex transport features (e.g., chemical reactions, convection, and turbulence coupling).

1. Introduction

Nuclear fusion energy has the potential to provide and satisfy the energy demand of being a game-changer for decarbonization, providing sustainability, affordability, and availability. However, nuclear fusion reactors are complex machines that have multiple engineering challenges to overcome. These machines usually rely on the Deuterium–Tritium (D–T) reaction due to the lower energy threshold required for the fusion to occur. The natural scarcity of T in nature requires its production *in situ* through the nuclear reaction between neutrons, which are emitted by the nuclear fusion reactor itself, and Lithium, in the tritium breeder component.

In particular, T breeding represents a tough challenge to overcome, with a design space bounded by the magnet geometry. Even with the addition of neutron multipliers (Pb, Be) and Li isotope reaction, the achievable Tritium Breeding Ratio (TBR) is slightly over unity. In the fuel cycle, extraction systems must retrieve as much produced T as retrievable, due to radiohazard and operational constraints, with an operational window for T losses smaller than $TBR - 1$. An increase in the retrieval efficiency and a decrease in T losses would increase the ability of the tokamak to withstand start-up transients, maintenance, and unscheduled interruptions of operations, and increase the reserve inventory build-up rate.

There are several challenges involving T handling in the reactor. Among suitable engineering components needed for the T circuit to work, the best-performing technology is yet to be identified. The evaluation of extraction rates, residence time, and T fluxes from the tritiated circuit is a fundamental insight to have when designing the reactor. Moreover, the great T exposure of plasma-facing components poses a great risk of high inventories and radioactive material if the material for these components is not chosen suitably. In this framework, T transport codes play a fundamental role in designing a nuclear fusion reactor and its tritiated circuit. While fuel cycle models exist [1–3], they would greatly benefit from detailed component-level information to improve their reliability. T transport codes are a versatile and indispensable tool to account for these crucial aspects and design an efficient T circuit. Moreover, T transport modeling is a crucial tool to evaluate

☆ This article is part of a Special issue entitled: 'PFMC-20' published in Nuclear Materials and Energy.

* Corresponding author.
E-mail address: raffaella.testoni@polito.it (R. Testoni).

https://doi.org/10.1016/j.nme.2025.102026
Received 26 June 2025; Received in revised form 4 November 2025; Accepted 7 November 2025
Available online 8 November 2025

the inventory, fluxes, and retention at the component level and to do a physics-informed design to choose the most reliable materials for structures, breeders, and plasma-facing components. In the last decade, multiple T transport codes have been developed to increase the capability of modeling diffusion processes for nuclear applications. One of the first applications is to estimate the T inventory in plasma-facing components [4–6], and fuel recycling and outgassing [6,7]. T transport codes are used to model and inform the multiple breeding blanket designs, such as solid breeders, LiPb-based technologies foreseen in DEMO [8], and FLiBe molten salt Liquid Immersion Blankets foreseen for ARC-class reactors [9–13]. Another focus is on T extraction technologies [14,15]. In addition, system-level codes for diffusion modeling have been developed for DEMO [16] and molten salt circuits [12,17]. Moreover, the focus of the nuclear fusion community has increasingly included breeding technologies and T technologies with experimental facilities [18–21]. Proper modeling of the trapping phenomena is relevant in these reactors due to the high thermal excursion foreseen in materials, the presence of Helium ashes that can interact with traps, the increase in empty trapping sites due to neutron damage, and the relevance of the trapping phenomenon during transients, such as start-ups.

The paper is structured as follows: Section 2 illustrates the physical equations to describe hydrogen transport with trapping. Then, Section 3 resumes the recent state of the art of H isotopes transport codes and their application in the nuclear fusion industry. Section 4 contains a series of verification cases (Section 4.1) for three different transport codes, MHIMS, FESTIM, and mHIT, and the results are compared against each other. The authors published an open-source repository on Github https://github.com/gabriele-ferrero/Titans_TT_codecomparison, containing the FESTIM and mHIT models, together with the scripts to make the plots for this paper. In Section 4.1.1, a 1D slab permeation without and with multiple traps verifies and compares the three codes on the diffusion and trapping modeling in 1D. Then, in Section 4.1.2, the Method of Manufactured Solutions [22,23] verifies for the mHIT code the transport equations in 2D, together with the concentration discontinuity happening at the interface between different materials. After the verification cases, Section 4.2 consists of three validation cases. In Section 4.2.1 and in Section 4.2.2 the three codes reproduce two different Thermal Desorption Spectroscopy (TDS) experiments [24,25] with excellent agreement. Then, in Section 4.2.3, the mHIT code is compared against FESTIM [5] to simulate and predict the T inventory in an ITER monoblock during a long transient. Section 5 summarizes the relevant results obtained through this study.

2. Physics of hydrogen isotopes transport

The diffusion of hydrogen isotopes (Q) is well described by Fick's diffusion laws (Eqs. (1) and (2)). The coupling between mobile Q and trapped Q is done through a volumetric source term ($\sum \frac{\partial c_{t,i}}{\partial t}$) in the mobile species equation, as depicted in Eq. (2). The Q density in traps can change due to mobile species moving into traps, and trapped species getting out from traps [26]. In the conditions of a single isotope and single occupancy for each trap site, the problem is described by Eq. (3):

$$J = -D\nabla c_m \tag{1}$$

$$\frac{\partial c_m}{\partial t} = \nabla \cdot (D\nabla c_m) + S - \sum \frac{\partial c_{t,i}}{\partial t} \tag{2}$$

$$\frac{\partial c_{t,i}}{\partial t} = k_i c_m (n_i - c_{t,i}) - p_i c_{t,i} \tag{3}$$

where J is the diffusive particle flux in [mol m^{-2} s^{-1}], D is the diffusion coefficient in [m^2 s^{-1}] and c_m is the mobile concentration of the species in [mol m^{-3}], S is a volumetric generation of the species [mol m^{-3} s−1], $c_{t,i}$ is the trapped concentration [mol m^{-3}] in the ith trap. k_i is the trapping rate in [m^3 mol^{-1} s^{-1}], n is the trap density [mol m^{-3}] of the ith trap in the material, p_i is the detrapping rate in [s^{-1}]. For the comparison carried out in this paper, the advection term, due to the fluid flow in which Q is dissolved, is neglected, and no case study with advection is presented. The main focus of the comparison carried out in this study is on the trapping physics, which is included in the three codes.

In the case of a dissociative surface, the surface flux for Q can be described through recombination and dissociation, following Eqs. (4) and (5):

$$J \cdot \mathbf{n} = K_r(T) c_m^2 \tag{4}$$

$$J \cdot \mathbf{n} = K_d(T) P_{Q_2} \tag{5}$$

where $\mathbf{n}$ is the normal vector to the boundary, K_r is the recombination coefficient in [m^4 mol^{-1} s^{-1}], K_d is the dissociation coefficient in [mol s^{-1} m^{-2} Pa] and P_{Q_2} is Q partial pressure in [Pa]. In a steady state, there is an equilibrium between the dissociation and recombination effects, and the concentration on the material surface is dependent on the Q partial pressure [27]. In the materials in which Q is dissolved in atomic form, Sieverts' law applies (Eq. (6)). It is the case for metals, for instance. In materials in which Q species are dissolved as molecules, Henry's law applies (Eq. (7)). In that case, there is no dissociation/recombination on the surface. It can be the case for molten salt, gases [28]. When two materials are in contact with each other, assuming the kinetic interface effects quickly reach a steady-state, the continuity of partial pressure is reached [29]. This phenomenon leads to discontinuities in the concentration profile, and it is handled differently between FESTIM and mHIT, which can handle multi-material scenarios. In FESTIM, when multiple materials are involved, the diffusion equations are solved for the partial pressure, with continuity across different material interfaces, and reconverted to concentration in post-processing. In mHIT, the equation to solve at the interface involves a partition condition $K_{+/-} = c^+/c^-$, being + and - the two domains across the interface. In a Sieverts/Sieverts interface K_{S^+/S^-} is evaluated through Eq. (10), while in a Henry/Sieverts interface, the continuity of the partial pressure is ensured through Eq. (11). The continuity of the Q flux is ensured on the Sieverts/Sieverts interface. However, in the Henry/Sieverts boundary, hydrogen is conserved by Eq. (12) because J_Q^+ is in the molar form Q_2, while J_S^- is in the atomic form Q [30]:

$$c_m = K_S \sqrt{P_{Q_2}} \tag{6}$$

$$c_m = K_H P_{Q_2} \tag{7}$$

$$K_S = \sqrt{K_d / K_r} \tag{8}$$

$$K_{H_s^{cp}} = \lim_{c_l \to 0} c_l / p \tag{9}$$

$$K_{S^+/S^-} = K_S^+(T)/K_S^-(T) \tag{10}$$

$$K_{H^+/S^-} = K_H^+ \, c^-/(K_S^-)^2 \tag{11}$$

$$J_H^+ = 0.5 J_S^- \tag{12}$$

where K_S (Eq. (8)) is the Sieverts' constant in [mol$_Q$ m^{-3} Pa$^{-0.5}$], and represents the equilibrium between dissociative flux (Eq. (5)) from the gas and recombinative flux (Eq. (4)) from the liquid. K_H or $K_{H_s^{cp}}$ is Henry's law solubility constant defined via concentration and partial pressure [31], in [mol$_{Q_2}$ m^{-3} Pa^{-1}]. The diffusivity, trapping rate, detrapping rate, recombination constant, dissociation constant, Sieverts constant, and Henry constant all follow an Arrhenius equation:

$$X(T) = X_0 e^{E_X/(k_B T)} \tag{13}$$

where X_0 is the pre-exponential factor and can be (D_0, k_0, p_0, $K_{r,0}$, $K_{d,0}$, $K_{S,0}$ and $K_{H,0}$, the activation energy E_X is in [eV] and can be

respectively E_D, E_k, E_p, E_r, E_{diss}, E_S and E_H, k_B is the Boltzmann constant and T is the temperature in [K]. As Q diffusion properties are significantly temperature dependent, the heat transfer equation is coupled weakly with Q diffusion:

$$\rho c_p \frac{\partial T}{\partial t} = \nabla \cdot (\lambda \nabla T) + \sum \dot{P} \tag{14}$$

being ρ the density in [$\mathrm{kg\,m^{-3}}$], c_p the heat capacity in [$\mathrm{J\,kg^{-1}\,K^{-1}}$], λ the thermal conductivity in [$\mathrm{W\,m^{-1}\,K^{-1}}$] and $\dot{P}$ the volumetric heat source in [$\mathrm{W\,m^{-3}}$]. For the applications in this paper, the advection term in the heat equation is neglected as it is not relevant to the presented case studies. The equations for Q transport (Eqs. (2) and (3)) are the same for each H isotope. However, a difference between different isotopes is in the diffusion coefficient, which is inversely proportional to the atom mass (Eq. (15)). This is particularly relevant for H isotopes, as the ratio of their isotopes is by far larger for light atoms than for heavy atoms.

$$D_Q = \frac{D_H}{\sqrt{M_Q/M_H}} \tag{15}$$

being Q an isotope and M_Q the atomic mass of the isotope. Because of the dependence of the detrapping rate on Q diffusivity, the detrapping and trapping pre-exponentials must be corrected by the same modification factor.

$$p_{0,Q} = \frac{D_{0,Q}}{\lambda^2} = \frac{p_{0,H}}{\sqrt{M_Q/M_H}} \tag{16}$$

$$k_{0,Q} = \frac{D_{0,Q}}{n_{IS}\lambda^2} = \frac{k_{0,H}}{\sqrt{M_Q/M_H}} \tag{17}$$

where n_{IS} is the density of interstitial sites in the lattice in $\mathrm{m^{-3}}$ and λ is the distance between two neighboring sites in m [32]. No relevant studies in the literature show solubility differences between different H isotopes. Other isotopic effects to account for are the isotopic exchange, H-driven T permeation, and account for the competition of different isotopes for the same trap sites in multi-isotopic diffusion; however, there are no modeling efforts yet to simulate these conditions that the authors are aware of.

3. Codes for hydrogen isotopes transport at the component level

In the nuclear industry, Q transport codes have been developed to simulate T diffusion in fission and fusion reactors, with a focus on Molten salt reactors from the fission industry. While the codes have been developed for T transport, they currently have more applications on H or D transport, as these isotopes are commonly employed in experiments, instead of the precious and scarce T.

TMAP (Tritium Migration Analysis Program) [33–35] is a MOOSE application for solving 3D diffusion of Q species, and it has been widely employed over the years for fusion applications. Currently in its TMAP8 version, the code is fully available open source at https://github.com/idaholab/TMAP8. While various Q transport codes have been developed to improve the capacity to simulate transport, TMAP is the most long-lived code, and its community is still active, with a recent publication of V&V benchmark for its code [36].

The transport code MHIMS was first introduced in [37–39]. Some applications of the MHIMS code include estimation of retention in tungsten monoblocks, ITER inventory estimation [4], TDS on tungsten [38] and EUROFER [25], with activation energy fitting [40], and kinetic surface modeling [41,42]. MHIMS uses the DLSODE package [43,44] to solve numerically the system of equations, and is applied in 1D problems.

FESTIM (Finite Elements Simulation of Tritium In Materials) [5,45,46] is an open-source tool for modeling Q transport with trapping effect. It leverages the FEniCS/DOLPHINx [47] computing platform to solve PDEs with the finite element method. The FESTIM suite is a flexible and transparent interface of FEniCS and DOLPHINx based on Python, and it is available as open source code at https://github.com/FESTIM-dev/FESTIM, with a currently active community. As FESTIM can simulate up to 3D geometries, it relies on different third-party software for mesh generation, such as the open-source SALOME mesher https://www.salome-platform.org/ or the gmsh Python package. The code has been employed to simulate TDS experiments [45], parametric analysis for activation energy fitting [48], estimate the tritium inventory in ITER monoblocks [5,29,49,50], and the evaluation of tritium inventory in the WCLL breeding blanket with computational fluid dynamics coupling in laminar flow regime [51].

The mHIT code is a set of added equations on top of the COMSOL® [52] chemical module. A suite of verification and validation benchmarks has been carried out for 1D cases [53]. The same environment without trapping effects has been employed for the numerical analysis in [27] and for the analysis of the WCLL tritium inventory [54,55]. The exploitation of the COMSOL modules suite permits geometry manipulation, meshing, multiphysics coupling of Q diffusion and trapping with heat transfer, fluid dynamics, turbulence effects, chemical reaction, and electric currents with ease.

4. Modeling and results

4.1. Verification benchmarks

4.1.1. Diffusion in an infinite-length slab

The first verification benchmark involves the Fickian diffusion Eqs. (1) and (2) on an infinite-length slab with a fixed concentration on both sides. On the left side, the concentration c_0 is 0.0088 mol $\mathrm{m^{-3}}$, and on the right side is 0, which assumes that Q recombines to Q_2 at a very fast rate. The computational domain is a 1D segment of finite thickness. First, a verification of the diffusion process without trapping phenomena is carried out. Then, traps are introduced with 3 different detrapping energies E_p, whose strength is measured through the trapping parameter ζ [56] and the trap filling ratio r [32,39,45] (Eqs. (18) and (19)). In particular, the trapping parameter $\zeta = \frac{c_m}{c_t}$ when Eqs. (2) and (3) are in steady state, and the trap filling ratio $r = \frac{c_{t,i}}{n_{t,i}}$ represents the fraction of filled trap sites:

$$\zeta = p(T)/(k(T)n) + c_0/n \tag{18}$$

$$r = (p(T)/(k(T)\,c_0) + 1)^{-1} \tag{19}$$

a weak trap of 1 eV ($\zeta = 0.56 \gg c_m/n$, $r = 1.5 \times 10^{-4}$), a strong trap of 2 eV ($\zeta - c_m/n = 5.1 \times 10^{-6}$, $r = 0.94$), and an irreversible trap of 2.5 eV ($\zeta - c_m/n = 1.54 \times 10^{-8}$, $r = 0.9999$). All trapping parameters are depicted in Table 1. The indicator parameter to compare results in this scenario is the Q flux on the right of the slab ($c = 0$). Results show good agreement between the analytical result and the codes for Q transport for the pure diffusion, weak trap, and intermediate trap scenarios from [56] (Fig. 1). It can be observed that the characteristic time for the flux to reach a steady state is significantly affected by the presence of the trap and its detrapping energy, showing a different increase of 3 orders of magnitude between the "weak" and the "medium" trap scenarios. This is expected in the limit $\zeta \gg c_m/n$, which indicates a low filling ratio. Therefore, in the "weak" trap, the diffusion of the species is similar to the diffusion as if there were no traps. In Fig. 1, there is a sensible difference between the "no trap" and "weak" trap scenarios, which is nowhere near the difference in the presence of stronger traps.

In the irreversible trap scenario, different behavior of the permeation can be observed: the Q atoms diffusing across the slab get immediately captured by empty traps before being able to diffuse past them, until there are no empty traps to fill, as expected with a filling ratio of $r \approx 1$. This creates the presence of a diffusion front in time, and a step profile in the concentration of filled traps in space, each time step until every empty trap site is filled in the entire slab. When this happens, the permeation flux on the other surface of the slab rises in a

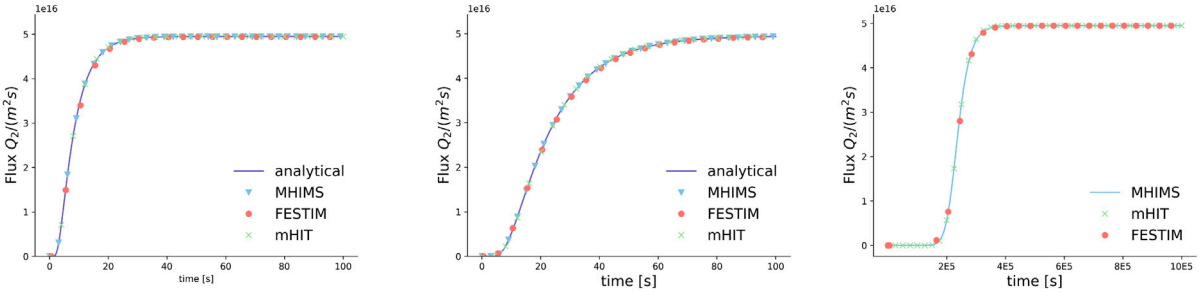

Fig. 1. Diffusion in an infinite-length slab - Q permeation across a slab with a constant concentration on one side. (a) No traps (b) Weak trap (c) Medium trap. Subplot (c) has a different scale for the time axis.

Table 1
Parameters for 1D slab benchmarks.

Parameter	Value	Unit
c_0	8.8×10^{-3}	mol m^{-3}
$thickness$	1	mm
p_0	10^{13}	s^{-1}
k_0	1.58×10^{7}	mol m^{-3} s^{-1}
E_D	0.2	eV
$E_p = E_{weak}$	1	eV
$E_p = E_{medium}$	2	eV
$E_p = E_{strong}$	2.5	eV
D_0	1.9×10^{-7}	m^2 s^{-1}
n_{trap}	$10^{-3} \times \rho_m$	mol m^{-3}
ρ_m	6.338×10^{28}	m^{-3}
T	1000	K

very short time from 0 to steady-state as there were no traps (Fig. 2). The comparison between the analytical results and the 3 codes shows a very good agreement, as the breakthrough time coincides, despite the shock-like behavior of the trap filling and permeation in this scenario.

4.1.2. Method of manufactured solutions

A verification study on transport phenomena and the interface boundary condition has been carried out with the Method of Manufactured Solutions (MMS) [22,23]. The MMS is a procedure for generating a numerical problem to verify codes and assess their accuracy. It consists of manufacturing an exact analytical solution for the problem, which does not need to have a physical meaning, and calculating the corresponding source term analytically. Then, the source term is applied to the computational domain in the model, together with coherent initial and boundary conditions. If the code is accurate, the exact analytical solution will be computed across the whole domain as a consequence of the source term, and the accuracy of the code can be quantified. This scenario involves a 2D time-dependent transport simulation with no traps. Other verifications on stationary and 1D conditions have been carried out, but only the most complex scenario is reported in this study. The analytical solutions, together with the source term used as input in mHIT, for this verification case, are listed in Table 2 and are plotted in Figs. 3–6. The FESTIM code has been verified with the same method in [29,57]. The analytical solution has been employed as a Dirichlet boundary condition in the mHIT model, and together with the source term is the driver term that will result in the analytical solution for the mHIT model. Two interface conditions, in the form of partition conditions, have been tested. For the Sieverts/Sieverts interface, a partition condition K = 10 has been employed. For the Henry/Sieverts interface, a partition condition of $K = 10 \times c^-$, so that $c^+ = K\, c^- = 10\, (c^-)^2$ has been employed. An excellent agreement between the analytical solution and the computed solution has been obtained, as depicted for the mobile concentration in Figs. 3 and 4, and for the trapped concentration in Figs. 5 and 6.

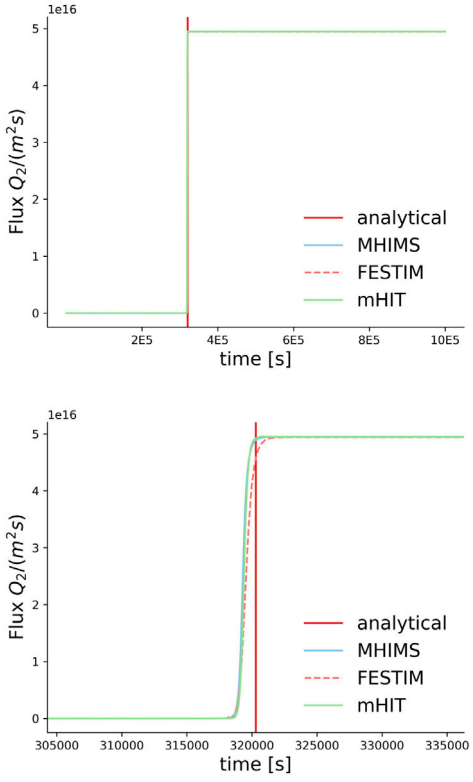

Fig. 2. Diffusion in an infinite-length slab - (a) Q permeation across a slab with constant concentration on one side and an irreversible trap. (b) Zoom magnification to observe the fast rise in the permeation flux.

4.2. Validation benchmarks

4.2.1. TDS experiment in tungsten

The two validation cases for the three codes consist of two benchmarks with experimental data from TDS experiments. A TDS experiment consists of exposing a material sample to a controlled environment with a hydrogen source (gas, ions, or plasma) to load up its traps. After the initial exposure, the sample is moved into an atmosphere without hydrogen, and the mobile hydrogen in the sample diffuses out, ideally leaving only the hydrogen in the traps in the sample. Then the sample is heated following a linear temperature increase while measuring the Q isotope outflux escaped from the traps. To reconstruct and simulate a TDS experiment, all these steps must be accounted for as the loaded trap profile is significantly dependent on previous exposure and resting conditions.

As a control parameter to compare the results, the hydrogen isotope flux depending on the temperature has been employed, which is a characteristic curve typical of TDS experiments. A peculiarity of this curve

Table 2
The solution function and source function used for MMS verification.

Interface	Material 1	Material 2
Sieverts/Sieverts mobile	$c_{m,an,1} = (1 + \cos(2\pi x)\cos(2\pi y))t$	$c_{m,an,2}(1 + \cos(2\pi x)\cos(2\pi y))tK$
Source Sieverts/Sieverts	$D \times (8\pi^2 t \cos(2\pi x)\cos(2\pi y) + \cos(2\pi x)\cos(2\pi y) + 1)$	$D\times(8K\pi^2 t \cos(2\pi x)\cos(2\pi y)+\cos(2\pi x)\cos(2\pi y)+1)$
Sieverts/Henry mobile	$(2 + \cos(2\pi x)\cos(2\pi y))t$	$((2 + \cos(2\pi x)\cos(2\pi y))t)^2 K$
Source Sieverts/Henry	$D \times (8\pi^2 t \cos(2\pi x)\cos(2\pi y) + \cos(2\pi x)\cos(2\pi y) + 2)$	$D \times (16K\pi^2 t^2(\cos(2\pi x)\cos(2\pi y) + 2\cos(2\pi x)\cos(2\pi y) - 8K\pi^2 t^2 \sin(2\pi x)^2 \cos(2\pi y)^2 - 8K\pi^2 t^2 \sin(2\pi y)^2 \cos(2\pi x)^2 + 2Kt(\cos(2\pi x)\cos(2\pi y) + 2)^2))$
Trapped solution	$\left(c_{t,in} - \frac{kc_{m,an,i}n}{kc_{m,an,i}+p}\right) e^{-(kc_{m,an,i}+p)t} + \frac{kc_{m,an,i}n}{kc_{m,an,i}+p}$	

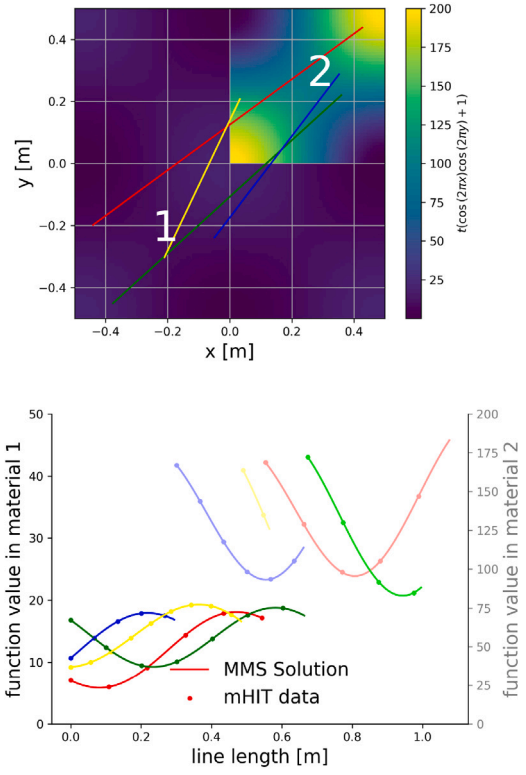

Fig. 3. Methods of Manufactured solutions - MMS verification for partition condition involving two Sieverts' constant materials. (a) Solution plot and random verification lines. (b) confrontation between mHIT and analytical solution on the random verification lines plotted in (a).

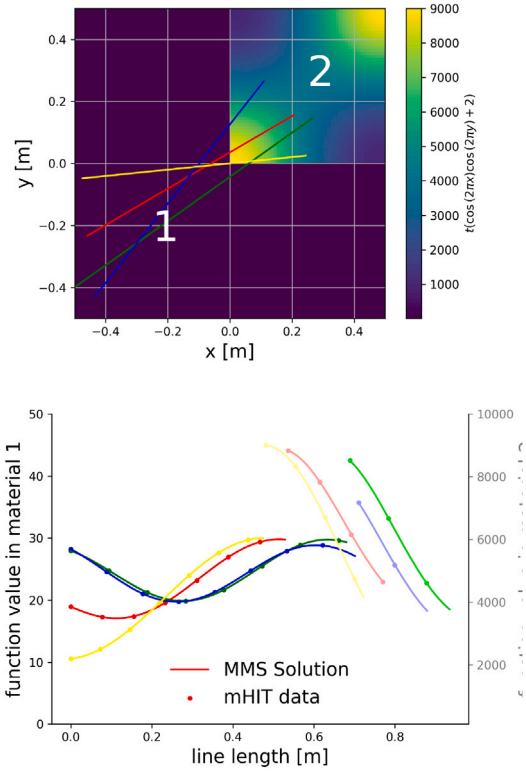

Fig. 4. Methods of Manufactured solutions - MMS verification for partition condition involving Sieverts' and Henry's constant materials. (a) Solution plot and randomly sampled verification lines. (b) confrontation between mHIT and analytical solution on the verification lines plotted in (a).

is that peaks are centered near the temperatures where Q release from the trap increases substantially. These temperature peaks are related to the characteristic detrapping energy of traps in the material. However, there are other transports to account for, such as bulk diffusion, which can delay the hydrogen isotope release. Therefore, the full simulation of the TDS and parametric fittings to evaluate E_p through these experiments is needed. Another approach to evaluate the detrapping energy E_p is through density functional theory calculations [58–62]. The 3 codes demonstrated good capability to reconstruct experimental results as depicted in Figs. 7 and 8. Tungsten (W) properties used in the first validation case [24] are listed for the reader's convenience in Table 3. Trap densities and energies have been obtained through an optimization with MHIMS with a relative error of 2.91%.

Table 3
Parameters for tungsten TDS.

Parameter	Value	Unit
D_0	$1.9/\sqrt{2}\times 10^{-7}$	$m^2\ s^{-1}$
p_0	10^{13}	s^{-1}
k_0	$10^{13}/(6\ \rho_W)$	$m^3\ mol^{-1}\ s^{-1}$
E_D	0.2	eV
E_1	0.834	eV
E_2	0.959	eV
E_3	1.496	eV
n_1	$1.364\times 10^{-3}\rho_W$	$mol\ m^{-3}$
n_2	$3.639\times 10^{-3}\rho_W$	$mol\ m^{-3}$
n_3	$9.742\times 10^{-2}\rho_W \times f(x)$	$mol\ m^{-3}$
ρ_W	6.388×10^{28}	m^{-3}

4.2.2. TDS experiment in EUROFER

The TDS experiment described in [25] is the last validation and comparison benchmark between MHIMS, FESTIM, and mHIT. In particular, for this study, we develop the FESTIM and mHIT model to compare against the MHIMS results. The experiment run consists of 2 different TDS curves, as during the first temperature ramp-up up the sample did not release all its trapped Q content, needing another temperature ramp-up to reach higher temperatures. All the experimental

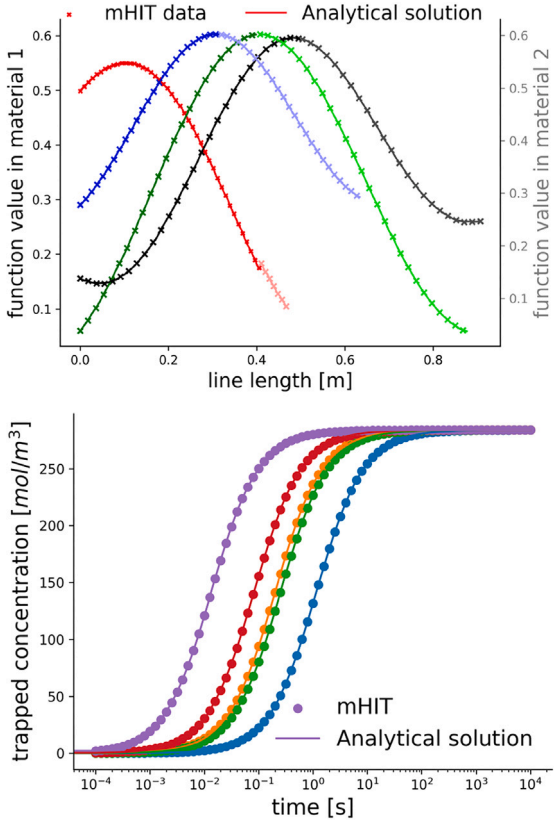

Fig. 5. Trapped concentration in the MMS verification study for the partition condition involving two Sieverts' constant materials. (a) Solution plot and random verification lines at $t = 10$ s. (b) confrontation between the transient evolution in mHIT and analytical solution on five random verification points on both materials.

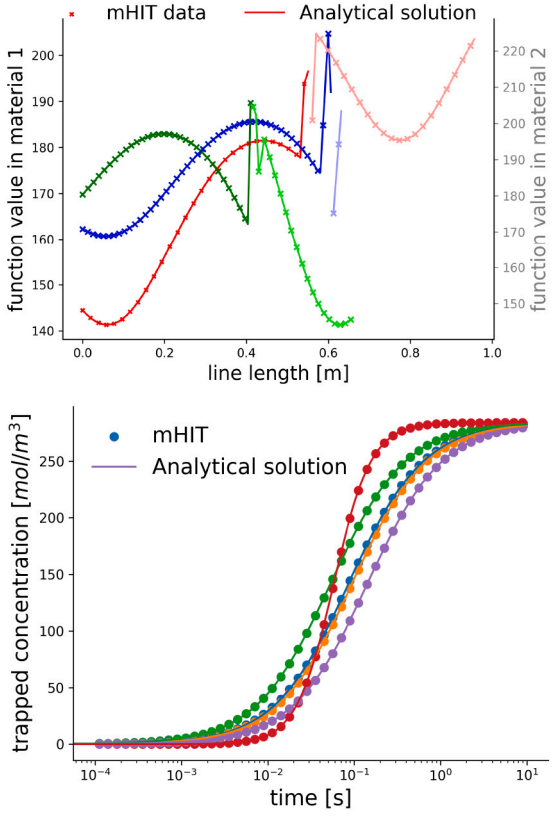

Fig. 6. Trapped concentration in the MMS verification study for Partition condition involving Sieverts' and Henry's constant materials. (a) Solution plot and random verification lines at $t = 10$ s. (b) confrontation between the transient evolution in mHIT and analytical solution on five random verification points on both materials.

Table 4
Parameters for EUROFER TDS.

Parameter	Value	Unit
D_0	$2.52/\sqrt{2} \times 10^{-7}$	$m^2\ s^{-1}$
p_0	10^{13}	s^{-1}
k_0	$10^{13}/(6\rho_W)$	$mol\ m^{-3}\ s^{-1}$
E_D	0.16	eV
E_1	0.51	eV
E_2	1.27	eV
E_3	1.65	eV
n_1	$7 \times 10^{-4}\rho_W$	$mol\ m^{-3}$
n_2	$7.49 \times 10^{-7}\rho_W$	$mol\ m^{-3}$
n_3	$4.517 \times 10^{-6}\rho_W$	$mol\ m^{-3}$
ρ_W	8.59×10^{28}	m^{-3}

conditions must be accounted for while simulating the TDS experiment, including the interruption and the second temperature ramp. Results in Fig. 8 depict very good agreement between the TDS spectra computed with the 3 codes, with a slightly higher flux on the first energy peak for mHIT. EUROFER trapping properties are listed in Table 4.

4.2.3. ITER monoblock 2D

The tritium inventory in the vacuum vessel must be minimized for multiple reasons:

- Safety reasons.
- The vacuum vessel is a tritium sink from the fuel cycle perspective and can affect its performance.
- Tritium outgassing from the vacuum vessel can decrease plasma performance [63].

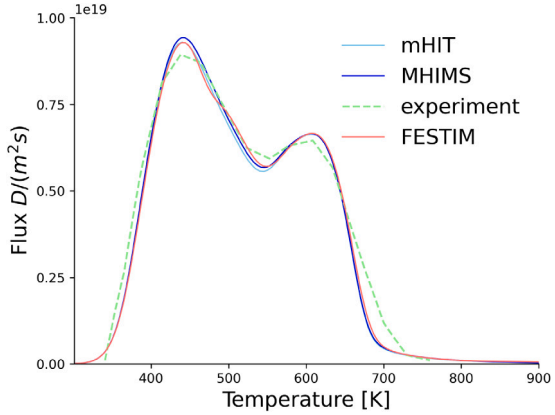

Fig. 7. TDS experiment in tungsten - Code comparison validation benchmark of TDS profile for tungsten.

- Tritium can deteriorate mechanical properties [64].

Tritium diffusion in the vacuum vessel can happen due to plasma tritium implantation in the divertor. The model to simulate an ITER monoblock has been reproduced in mHIT from the FESTIM model, described in [5,29,49,50].

The mHIT model is compared with the FESTIM model, available as an open-source repository. The material properties for the simulation are listed in Table 5. The tritium inventory in each material agrees well for the whole transient between FESTIM and mHIT (Fig. 10).

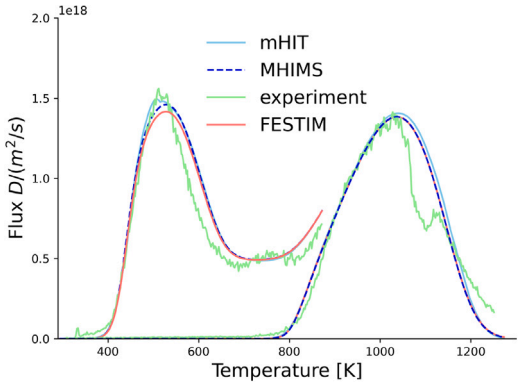

Fig. 8. TDS experiment in EUROFER - Code comparison validation benchmark of TDS profile for EUROFER.
Source: The MHIMS curve is reproduced from [25].

Table 5
Parameters for the ITER 2D simulation.

Parameter	Tungsten	Cu	CuCrZr	Unit
D_0	1.9×10^{-7}	6.6×10^{-7}	3.9×10^{-7}	$m^2\ s^{-1}$
S_0	$1.87 \times 10^{24}/N_A$	$3.14 \times 10^{24}/N_A$	$4.28 \times 10^{28}/N_A$	$mol_Q\ m^{-3}\ Pa^{-0.5}$
p_0	10^{13}	8×10^{13}	8×10^{13}	s^{-1}
k_0	$8.96 \times 10^{-17} N_A$	$6 \times 10^{-17} N_A$	$1.2 \times 10^{-16} N_A$	$mol\ m^{-3}\ s^{-1}$
E_D	0.2	0.39	0.42	eV
E_S	1.04	0.57	0.39	eV
E_k	0.2	0.39	0.42	eV
E_p	0.87	0.5	0.85	eV
$E_{p,2}$	1	–	–	eV
n_1	$1.1 \times 10^{-3} \rho_W$	$5 \times 10^{-5} \rho_{Cu}$	$5 \times 10^{-5} \rho_{CuCrZr}$	$mol\ m^{-3}$
n_2	$4 \times 10^{-4} \rho_W$	–	–	$mol\ m^{-3}$
ρ	$6.28 \times 10^{28}/N_A$	$8.43 \times 10^{28}/N_A$	$2.61 \times 10^{28}/N_A$	$mol\ m^{-3}$

Trapped and mobile tritium distribution in the monoblock agrees well during the transient, and the mHIT result is depicted in Fig. 9, together with the temperature distribution. Mobile tritium is most present in the copper after it is allowed to permeate through the monoblock and reach the inner pipe layer. The trapped tritium distribution is the result of temperature distribution, mobile concentration, and time-dependent regime. While mobile concentration is linked to trap concentrations, the location of the maximum concentration of trapped tritium does not exactly coincide with the location of the mobile maximum, due to the Temperature being colder on the bottom boundary of the monoblock. The regime has not reached a steady state yet, and trapped tritium can reach higher concentrations in colder regions as time goes on. As a means of comparison between mHIT and FESTIM, the tritium concentration distribution on a projection line of the monoblock, which includes all materials, is displayed in Fig. 11, and depicts very good agreement between the two codes.

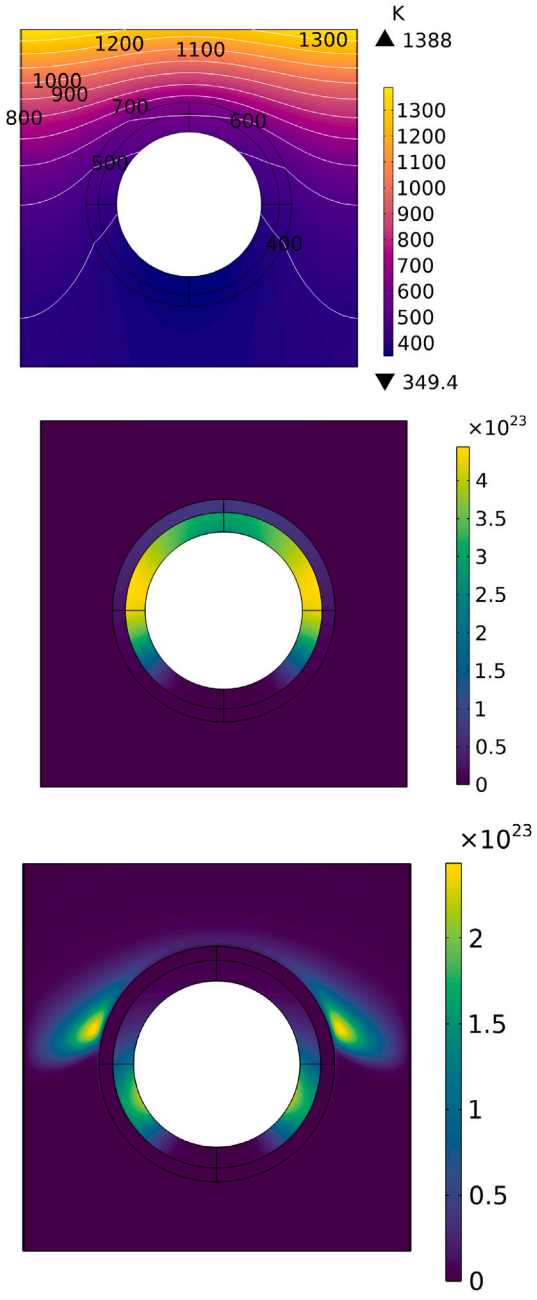

Fig. 9. ITER Monoblock 2D - Temperature and tritium distribution evaluated with mHIT in an ITER monoblock represented in 2D after $10^7 s$ (a) Temperature (b) Mobile tritium (c) Trapped tritium.

5. Conclusion

In recent years, hydrogen isotopes transport capability has improved with multiple transport codes. In this framework, the extensive comparison carried out in this work shows the capability of three different codes to solve Q transport in multiple scenarios. The comparison between the codes shows a good agreement in each of the selected benchmarks. While some extra features are characteristic of each code, having a common and tested base in the diffusion-limited regime and trapping equation leaves the user the possibility to choose whichever software to employ for component-level modeling based on its accessibility and its needs.

Different codes address the modeling needs for a wide range of case studies. MHIMS is capable of surface effects modeling for 1D scenarios, while FESTIM is open-source software that can handle up to 3 dimensions, multi-material, has great customizability and flexibility, and can couple laminar flow and heat transfer in Q transport. With this work, the code mHIT is extensively verified, validated, and compared against previously tested Q transport codes for multi-dimensional and multi-material transients, and its multiphysics characteristic can be exploited to increase the modeling capabilities for H-transport. Moreover, each of these codes can benefit from the other, due to multiple similarities shared between them, which can be leveraged for upgrades and further testing suites. This can be the case for surface modeling, convective transport term, and coupling between transport and turbulence fluid dynamics wall boundary conditions.

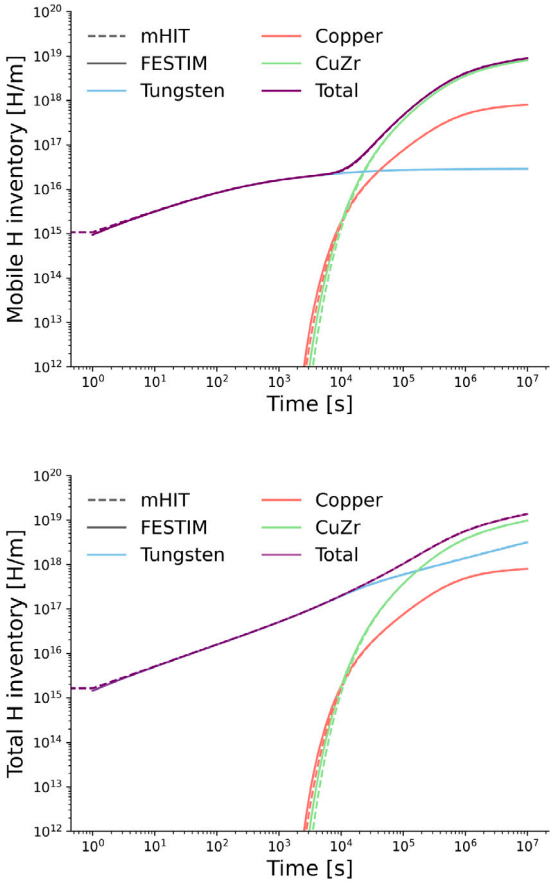

Fig. 10. ITER Monoblock 2D - Comparison of inventory evolution in time for ITER 2D validation scenario. (a) mobile inventory (b) total inventory (trapped+mobile).
Source: FESTIM simulations are reproduced from [45].

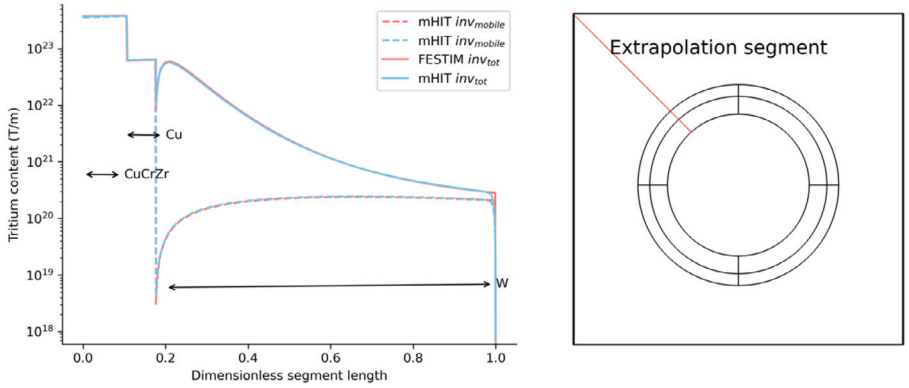

Fig. 11. Spatial distribution(left) of tritium content in the ITER plasma facing component projected on the extrapolation line (right).

CRediT authorship contribution statement

Gabriele Ferrero: Writing – review & editing, Writing – original draft, Visualization, Validation, Software, Methodology, Investigation, Formal analysis, Data curation, Conceptualization. **Raffaella Testoni:** Writing – review & editing, Writing – original draft, Validation, Supervision, Project administration, Methodology, Funding acquisition, Formal analysis, Data curation, Conceptualization. **Etienne A. Hodille:** Validation, Supervision, Software, Resources, Methodology, Investigation, Funding acquisition, Formal analysis.

Declaration of competing interest

The authors declare the following financial interests/personal relationships which may be considered as potential competing interests: Gabriele Ferrero reports financial support was provided by European Union. Raffaella Testoni reports financial support was provided by European Union. Gabriele Ferrero reports financial support was provided by Ministry of University and Research. If there are other authors, they declare that they have no known competing financial interests or

personal relationships that could have appeared to influence the work reported in this paper.

Acknowledgments

The work of G. Ferrero is financially supported by FSE REACT-EU-PON Ricerca e Innovazione 2014–2020, DM 1061/2021.

This work has been carried out within the framework of the TITANS project and has received funding from the European Commission 2022–2025 under grant agreement No 101059408. Views and opinions expressed are however those of the author(s) only and do not necessarily reflect those of the European Union or the European Atomic Energy Community ('EC-Euratom'). Neither the European Union nor the granting authority can be held responsible for them.

Data availability

The data and the analysis is available in the open source repository https://github.com/gabriele-ferrero/Titans_TT_codecomparison.

References

[1] M. Abdou, M. Riva, A. Ying, C. Day, A. Loarte, L. Baylor, P. Humrickhouse, T.F. Fuerst, S. Cho, Physics and technology considerations for the deuterium–tritium fuel cycle and conditions for tritium fuel self sufficiency, Nucl. Fusion 61 (1) (2020) 013001.

[2] S. Meschini, S.E. Ferry, R. Delaporte-Mathurin, D.G. Whyte, Modeling and analysis of the tritium fuel cycle for ARC-and STEP-class DT fusion power plants, Nucl. Fusion 63 (12) (2023) 126005.

[3] S. Meschini, R. Delaporte-Mathurin, G.R. Tynan, S. Ferry, Impact of trapping on tritium self-sufficiency and tritium inventories in fusion power plant fuel cycles, Nucl. Fusion (2025).

[4] E.A. Hodille, E. Bernard, S. Markelj, J. Mougenot, C.S. Becquart, R. Bisson, C. Grisolia, Estimation of the tritium retention in ITER tungsten divertor target using macroscopic rate equations simulations, Phys. Scr. 2017 (T170) (2017) 014033, http://dx.doi.org/10.1088/1402-4896/aa8787.

[5] R. Delaporte-Mathurin, E.A. Hodille, J. Mougenot, Y. Charles, C. Grisolia, Finite element analysis of hydrogen retention in ITER plasma facing components using FESTIM, Nucl. Mater. Energy 21 (2019) 100709.

[6] K. Schmid, Diffusion-trapping modelling of hydrogen recycling in tungsten under ELM-like heat loads, Phys. Scr. 2016 (T167) (2016) 014025.

[7] J. Denis, J. Bucalossi, G. Ciraolo, E. Hodille, B. Pégourié, H. Bufferand, C. Grisolia, T. Loarer, Y. Marandet, E. Serre, Dynamic modelling of local fuel inventory and desorption in the whole tokamak vacuum vessel for auto-consistent plasma-wall interaction simulations, Nucl. Mater. Energy 19 (2019) 550–557, http://dx.doi.org/10.1016/j.nme.2019.03.019, URL https://www.sciencedirect.com/science/article/pii/S235217911830262X.

[8] A. Del Nevo, E. Martelli, P. Agostini, P. Arena, G. Bongiovì, G. Caruso, G. Di Gironimo, P. Di Maio, M. Eboli, R. Giammusso, et al., WCLL breeding blanket design and integration for DEMO 2015: status and perspectives, Fusion Eng. Des. 124 (2017) 682–686.

[9] B.N. Sorbom, J. Ball, T.R. Palmer, F.J. Mangiarotti, J.M. Sierchio, P. Bonoli, C. Kasten, D.A. Sutherland, H.S. Barnard, C.B. Haakonsen, J. Goh, C. Sung, D.G. Whyte, ARC: A compact, high-field, fusion nuclear science facility and demonstration power plant with demountable magnets, Fusion Eng. Des. 100 (2015) 378–405, http://dx.doi.org/10.1016/j.fusengdes.2015.07.008, URL https://www.sciencedirect.com/science/article/pii/S0920379615302337.

[10] A. Kuang, N. Cao, A.J. Creely, C.A. Dennett, J. Hecla, B. LaBombard, R.A. Tinguely, E.A. Tolman, H. Hoffman, M. Major, et al., Conceptual design study for heat exhaust management in the ARC fusion pilot plant, Fusion Eng. Des. 137 (2018) 221–242.

[11] R. Arredondo, K. Schmid, I. Ricapito, A. Lukenskas, G. Spagnuolo, Preliminary assessment of tritium permeation and retention in the European water cooled lithium lead test blanket module with TESSIM-x, Nucl. Mater. Energy 32 (2022) 101228, http://dx.doi.org/10.1016/j.nme.2022.101228, URL https://www.sciencedirect.com/science/article/pii/S2352179122001090.

[12] J.D. Stempien, R.G. Ballinger, C.W. Forsberg, An integrated model of tritium transport and corrosion in fluoride salt-cooled high-temperature reactors (FHRs)–part I: Theory and benchmarking, Nucl. Eng. Des. 310 (2016) 258–272.

[13] G. Ferrero, S. Meschini, R. Testoni, A preliminary CFD and tritium transport analysis for ARC blanket, Fusion Sci. Technol. 78 (8) (2022) 617–630.

[14] D. Demange, R. Antunes, O. Borisevich, L. Frances, D. Rapisarda, A. Santucci, M. Utili, Tritium extraction technologies and DEMO requirements, Fusion Eng. Des. 109 (2016) 912–916.

[15] M. Utili, C. Alberghi, L. Candido, F. Papa, M. Tarantino, A. Venturini, TRIEX-II: an experimental facility for the characterization of the tritium extraction unit of the WCLL blanket of ITER and DEMO fusion reactors, Nucl. Fusion 62 (6) (2022) 066036.

[16] F.R. Urgorri, C. Moreno, E. Carella, J. Castellanos, A. Del Nevo, Á. Ibarra, Preliminary system modeling for the eurofusion water cooled lithium lead blanket, Fusion Sci. Technol. 71 (3) (2017) 444–449.

[17] J.D. Stempien, Tritium Transport, Corrosion, and Fuel Performance Modeling in the Fluoride Salt-Cooled High-Temperature Reactor (FHR) (Ph.D. thesis), Massachusetts Institute of Technology, 2015.

[18] S.E. Ferry, K.B. Woller, E.E. Peterson, C. Sorensen, D.G. Whyte, The LIBRA experiment: Investigating robust tritium accountancy in molten FLiBe exposed to a DT fusion neutron spectrum, Fusion Sci. Technol. 79 (1) (2023) 13–35.

[19] C.N. Taylor, T.F. Fuerst, R.J. Pawelko, M. Shimada, The tritium extraction experiment (TEX): A forced convection fusion blanket PbLi loop, Fusion Eng. Des. 192 (2023) 113737.

[20] S. Strikwerda, P.A. Staniec, M. Jong, B. Wakeling, S. Reynolds, I. Castillo, S. Suppiah, H. Boniface, D. Ryland, T. Whitehorne, et al., Tritium opportunities and challenges for fusion developments worldwide—CNL and UKAEA view, Fusion Sci. Technol. (2023) 1–9.

[21] S. Takeda, S. Ogawa, M. Tabuchi, Y. Kume, R. Pearson, C. Baus, S. Konishi, K.F.U. Team, UNITY: Kyoto fusioneering's unique integrated testing facility for fusion power generation, Fusion Sci. Technol. (2023) 1–6.

[22] B.D. Dudson, J. Madsen, J. Omotani, P. Hill, L. Easy, M. Løiten, Verification of BOUT++ by the method of manufactured solutions, Phys. Plasmas 23 (6) (2016) 062303, http://dx.doi.org/10.1063/1.4953429, _eprint: https://pubs.aip.org/aip/pop/article-pdf/doi/10.1063/1.4953429/15905581/062303_1_online.pdf.

[23] P.J. Roache, Code Verification by the Method of Manufactured Solutions, J. Fluids Eng. 124 (1) (2001) 4–10, http://dx.doi.org/10.1115/1.1436090, _eprint: https://asmedigitalcollection.asme.org/fluidsengineering/article-pdf/124/1/4/5901562/4_1.pdf.

[24] O.V. Ogorodnikova, J. Roth, M. Mayer, Deuterium retention in tungsten in dependence of the surface conditions, J. Nucl. Mater. 313–316 (2003) 469–477, http://dx.doi.org/10.1016/S0022-3115(02)01375-2, URL https://www.sciencedirect.com/science/article/pii/S0022311502013752.

[25] F. Montupet-Leblond, E. Hodille, M. Payet, R. Delaporte-Mathurin, E. Bernard, Y. Charles, J. Mougenot, S. Vartanian, C. Grisolia, Influence of traps reversibility on hydrogen permeation and retention in eurofer97, Nucl. Fusion 62 (8) (2022) 086011, http://dx.doi.org/10.1088/1741-4326/ac6e74.

[26] A. McNabb, P. Foster, A new analysis of diffusion of hydrogen in iron and ferritic steels, Trans. Metall. Soc. AIME 227 (3) (1963) 618.

[27] C. Alberghi, L. Candido, M. Utili, M. Zucchetti, Development of new analytical tools for tritium transport modelling, Fusion Eng. Des. 177 (2022) 113083.

[28] P.W. Humrickhouse, T.F. Fuerst, Tritium transport phenomena in molten-salt reactors, 2020, URL https://www.osti.gov/biblio/1777267.

[29] R. Delaporte-Mathurin, E.A. Hodille, J. Mougenot, Y. Charles, G. De Temmerman, F. Leblond, C. Grisolia, Influence of interface conditions on hydrogen transport studies, Nucl. Fusion 61 (3) (2021) 036038.

[30] T.F. Fuerst, C.N. Taylor, A.A. Riet, J.R. Redmond, S. Sharma, A. Bowers, T. Mui, Y. Mao, R. Hui, Molten salt tritium transport experiment: A versatile fluoride salt loop for validation of tritium transport phenomena, Tech. rep., 2023, URL https://www.osti.gov/biblio/2203243.

[31] R. Sander, W.E. Acree, A.D. Visscher, S.E. Schwartz, T.J. Wallington, Henry's law constants (IUPAC recommendations 2021), Pure Appl. Chem. 94 (1) (2022) 71–85, http://dx.doi.org/10.1515/pac-2020-0302.

[32] E. Hodille, Study and modeling of the deuterium trapping in ITER relevant materials (Ph.D. thesis), UNIVERSITE D'AIX-MARSEILLE, 2016.

[33] G.R. Longhurst, D. Holland, J. Jones, B. Merrill, TMAP4 Users Manual, Tech. rep., EG and G Idaho, Inc., Idaho Falls, ID (United States), 1992.

[34] A.D. Lindsay, TMAP8, 2021, http://dx.doi.org/10.11578/dc.20210205.2, Published: [Computer Software] https://doi.org/10.11578/dc.20210205.2.

[35] A.D. Lindsay, TMAP8, 2021, http://dx.doi.org/10.11578/dc.20210205.2, URL https://doi.org/10.11578/dc.20210205.2 [Computer Software].

[36] P.-C.A. Simon, C.T. Icenhour, G. Singh, A.D. Lindsay, C.V. Bhave, L. Yang, A.A. Riet, Y. Che, P. Humrickhouse, M. Shimada, P. Calderoni, MOOSE-based tritium migration analysis program, version 8 (TMAP8) for advanced open-source tritium transport and fuel cycle modeling, Fusion Eng. Des. 214 (2025) 114874, http://dx.doi.org/10.1016/j.fusengdes.2025.114874.

[37] X. Bonnin, E. Hodille, N. Ning, C. Sang, C. Grisolia, Rate equations modeling for hydrogen inventory studies during a real tokamak material thermal cycle, J. Nucl. Mater. 463 (2015) 970–973, http://dx.doi.org/10.1016/j.jnucmat.2014.10.053, URL https://www.sciencedirect.com/science/article/pii/S0022311514007375.

[38] E.A. Hodille, X. Bonnin, R. Bisson, T. Angot, C.S. Becquart, J.M. Layet, C. Grisolia, Macroscopic rate equation modeling of trapping/detrapping of hydrogen isotopes in tungsten materials, J. Nucl. Mater. 467 (2015) 424–431, http://dx.doi.org/10.1016/j.jnucmat.2015.06.041, URL https://www.sciencedirect.com/science/article/pii/S0022311515300660.

[39] E.A. Hodille, A. Založnik, S. Markelj, T. Schwarz-Selinger, C.S. Becquart, R. Bisson, C. Grisolia, Simulations of atomic deuterium exposure in self-damaged tungsten, Nucl. Fusion 57 (5) (2017) 056002, http://dx.doi.org/10.1088/1741-4326/aa5aa5, Publisher: IOP Publishing.

[40] F. Montupet-Leblond, L. Corso, M. Payet, R. Delaporte-Mathurin, E. Bernard, Y. Charles, J. Mougenot, S. Vartanian, E. Hodille, C. Grisolia, Permeation and trapping of hydrogen in eurofer97, Nucl. Mater. Energy 29 (2021) 101062, http://dx.doi.org/10.1016/j.nme.2021.101062, URL https://www.sciencedirect.com/science/article/pii/S2352179121001290.

[41] E. Hodille, S. Markelj, M. Pecovnik, M. Ajmalghan, Z. Piazza, Y. Ferro, T. Schwarz-Selinger, C. Grisolia, Kinetic model for hydrogen absorption in tungsten with coverage dependent surface mechanisms, Nucl. Fusion 60 (10) (2020) 106011, http://dx.doi.org/10.1088/1741-4326/aba454.

[42] F. Montupet-Leblond, E. Bernard, S. Feuillastre, S. Garcia-Argote, E. Hodille, M. Payet, C. Grisolia, Development of the water-interface permeation in tritium-exposed materials (wapiti) tritium experiment and preliminary eurofer97 results, Nucl. Mater. Energy 38 (2024) 101561.

[43] A.C. Hindmarsh, ODEPACK, a systemaized collection of ODE solvers, in: R.S. Stepleman (Ed.), Scientific Computing, in: IMACS Transactions on Scientific Computation, vol. 1, North Holland, Amsterdam, 1983, pp. 55–64.

[44] K. Radhakrishnan, A.C. Hindmarsh, Description and use of LSODE, the live-more solver for ordinary differential equations, 1993, http://dx.doi.org/10.2172/15013302.

[45] R. Delaporte-Mathurin, Hydrogen Transport in Tokamaks: estimation of the ITER Divertor Tritium Inventory and Influence of Helium Exposure (Ph.D. thesis), Université Paris-Nord-Paris XIII, 2022.

[46] R. Delaporte-Mathurin, J. Dark, G. Ferrero, E.A. Hodille, V. Kulagin, S. Meschini, FESTIM: An open-source code for hydrogen transport simulations, Int. J. Hydrog. Energy 63 (2024) 786–802, http://dx.doi.org/10.1016/j.ijhydene.2024.03.184, URL https://www.sciencedirect.com/science/article/pii/S0360319924010218.

[47] I.A. Baratta, J.P. Dean, J.S. Dokken, M. Habera, J.S. Hale, C.N. Richardson, M.E. Rognes, M.W. Scroggs, N. Sime, G.N. Wells, DOLFINx: the next generation FEniCS problem solving environment, 2023, http://dx.doi.org/10.5281/zenodo.10447666, preprint.

[48] R. Delaporte-Mathurin, E.A. Hodille, J. Mougenot, Y. Charles, C. Grisolia, Parametric optimisation based on TDS experiments for rapid and efficient identification of hydrogen transport materials properties, Nucl. Mater. Energy 27 (2021) 100984.

[49] R. Delaporte-Mathurin, R. Chochoy, J. Mougenot, Y. Charles, E.A. Hodille, C. Grisolia, 3D effects on hydrogen transport in ITER-like monoblocks, Nucl. Fusion 64 (2) (2023) 026003.

[50] R. Delaporte-Mathurin, E. Hodille, J. Mougenot, G. De Temmerman, Y. Charles, C. Grisolia, Parametric study of hydrogenic inventory in the ITER divertor based on machine learning, Sci. Rep. 10 (1) (2020) 17798.

[51] J. Dark, R. Delaporte-Mathurin, Y. Charles, E.A. Hodille, C. Grisolia, J. Mougenot, Influence of hydrogen trapping on WCLL breeding blanket performances, Nucl. Fusion 61 (11) (2021) 116076.

[52] C. Multiphysics, Introduction to COMSOL multiphysics®, in: COMSOL Multiphysics, Burlington, MA, 1998, p. 2018, (accessed Feb 9).

[53] L. Candido, C. Alberghi, Verification and validation of mHIT code over TMAP for hydrogen isotopes transport studies in fusion-relevant environments, Fusion Eng. Des. 172 (2021) 112740.

[54] L. Candido, C. Alberghi, F. Moro, S. Noce, R. Testoni, M. Utili, M. Zucchetti, A novel approach to the study of magnetohydrodynamic effect on tritium transport in WCLL breeding blanket of DEMO, Fusion Eng. Des. 167 (2021) 112334.

[55] C. Alberghi, L. Candido, R. Testoni, M. Utili, M. Zucchetti, Magneto-convective effect on tritium transport at breeder unit level for the WCLL breeding blanket of DEMO, Fusion Eng. Des. 160 (2020) 111996.

[56] G.R. Longhurst, J. Ambrosek, Verification and Validation of the Tritium Transport Code TMAP7, Fusion Sci. Technol. 48 (1) (2005) 468–471, http://dx.doi.org/10.13182/FST05-A967, Publisher: Taylor & Francis _eprint: https://doi.org/10.13182/FST05-A967.

[57] R. Delaporte-Mathurin, J. Santana, FESTIM v&v book, 2024.

[58] A.D. Backer, D.R. Mason, C. Domain, D. Nguyen-Manh, M.-C. Marinica, L. Ventelon, C.S. Becquart, S.L. Dudarev, Hydrogen accumulation around dislocation loops and edge dislocations: from atomistic to mesoscopic scales in BCC tungsten, Phys. Scr. 2017 (T170) (2017) 014073, http://dx.doi.org/10.1088/1402-4896/aa9400, Publisher: IOP Publishing.

[59] A.D. Backer, D.R. Mason, C. Domain, D. Nguyen-Manh, M.-C. Marinica, L. Ventelon, C.S. Becquart, S.L. Dudarev, Multiscale modelling of the interaction of hydrogen with interstitial defects and dislocations in BCC tungsten, Nucl. Fusion 58 (1) (2017) 016006, http://dx.doi.org/10.1088/1741-4326/aa8e0c, Publisher: IOP Publishing.

[60] K. Heinola, T. Ahlgren, K. Nordlund, J. Keinonen, Hydrogen interaction with point defects in tungsten, Phys. Rev. B 82 (9) (2010) 094102, http://dx.doi.org/10.1103/PhysRevB.82.094102, URL https://link.aps.org/doi/10.1103/PhysRevB.82.094102 Publisher: American Physical Society.

[61] G.-H. Lu, H.-B. Zhou, C.S. Becquart, A review of modelling and simulation of hydrogen behaviour in tungsten at different scales, Nucl. Fusion 54 (8) (2014) 086001, http://dx.doi.org/10.1088/0029-5515/54/8/086001, Publisher: IOP Publishing.

[62] H.-B. Zhou, Y.-L. Liu, S. Jin, Y. Zhang, G.-N. Luo, G.-H. Lu, Investigating behaviours of hydrogen in a tungsten grain boundary by first principles: from dissolution and diffusion to a trapping mechanism, Nucl. Fusion 50 (2) (2010) 025016, http://dx.doi.org/10.1088/0029-5515/50/2/025016.

[63] C. Grisolia, T.S. team, et al., Plasma wall interaction during long pulse operation in tore supra, J. Nucl. Mater. 266 (1999) 146–152.

[64] S.K. Dwivedi, M. Vishwakarma, Hydrogen embrittlement in different materials: A review, Int. J. Hydrog. Energy 43 (46) (2018) 21603–21616.